*J. Fluid Mech.* (1990), *vol.* 219, *pp.* 449–468
*Printed in Great Britain*



# Stability of an oscillated fluid with a uniform density gradient

By DAVID JACQMIN
NASA Lewis Research Center, Cleveland, OH 44135, USA

(Received 6 March 1989)

We consider instabilities in a fluid with a constant density gradient that is subject to arbitrarily oriented oscillatory accelerations. With the Boussinesq approximation and for the case of an unbounded fluid, transformation to Lagrangian coordinates allows the reduction of the problem to an ordinary differential equation for each three-dimensional wavenumber. The problem has three parameters: the non-dimensional amplitude $R$ of the base-state oscillation, the non-dimensional level of background steady acceleration, which for some cases can be represented in terms of a local (in time) Richardson number $Ri$, and the Prandtl number $Pr$. Some general bounds on stability are derived. For $Pr = 1$ closed-form solutions are found for impulse (delta function) accelerations and a general asymptotic solution is constructed for large $R$ and general imposed accelerations. The asymptotic solution takes advantage of the fact that at large $R$ wave growth is concentrated at 'zero points'. These are times when the effective vertical wavenumber passes through zero. Kelvin–Helmholtz instabilities are found to dominate at low $R$ while Rayleigh–Taylor instabilities dominate at high. At high $R$, the uniform shear of the Kelvin–Helmholtz case tends to distort and weaken instability waves. With unsteady flows, $Ri = \frac{1}{4}$ is no longer an instability limit. Significant instabilities have been found for sinusoidal forcing for $Ri$ up to 0.6.

## 1. Introduction

There has been considerable interest recently in examining the response of non-homogeneous fluids to oscillating accelerations. Most effort has been directed toward convection induced by accelerations directed parallel to the fluid's density gradient. Recent work, for example, has been reported by Wadih & Roux (1988), who considered the onset of convection in an infinite cylinder with the temperature gradient and accelerations directed along its length. Earlier work has been reported by Donnelly, Reif & Suhl (1962), Gresho & Sani (1970), and Burde (1970). In contrast, there has been no analytically oriented work done for the apparently more important case (Kamotani, Prasad & Ostrach 1978) of the density gradient and accelerations oriented normally to each other. This orientation directly excites fluid motion and would seem therefore to offer the possibility of very rapid growth of instabilities.

The reason for the neglect is the very reason why it is interesting: the oscillating convective terms caused by the acceleration add considerable difficulties to a convectional linearized analysis. However, there is one situation in which these difficulties can be overcome; that is when a uniform density gradient causes an approximately uniform shear flow. With uniform shear a Lagrangian coordinate

transformation can eliminate the spatial dependence of the linearized equations' coefficients. Further, if the scale of excited instabilities is smaller than the width of the shear region, it may be acceptable to model the shear as unbounded. This then permits a reduction of the problem to the solution of ordinary differential equations with time-dependent coefficients. The usefulness of the Lagrangian transformation for uniform shear problems was first noticed by Lord Kelvin (Thomson 1877) but it was largely forgotten until the last two decades. The technique has been recently used by Hartman (1975), Marcus & Press (1977), Tung (1983), Lagnado, Phan-Thien & Leal (1984), Bayley (1986), Landman & Saffman (1987), Craik (1989), and Farrell (1989). Craik & Criminale (1986) give a thorough discussion of instabilities of a wide variety of non-parallel shear flows.

The paper proceeds as follows. The perturbation flow equations for unbounded, oscillating shear are derived in §2. Qualitative features of Rayleigh–Taylor instabilities are discussed briefly in §3. The Kelvin–Helmholtz case with zero mean acceleration is discussed in §4. For $Pr = 1$ exact closed-form solutions are derived for the case of impulse forcing, and asymptotic solutions are derived for general forcing at large $R$. These are used to discuss the qualitative features of the Kelvin–Helmholtz instabilities. The modifying effects of a mean stabilizing acceleration are then discussed in §5. Concluding comments along with a brief discussion of the effects of boundaries are contained in §6.

## 2. Formulation

We consider an unbounded Boussinesq fluid subject to periodic accelerations. Cartesian coordinates $\{x, y, z\}$ are used with corresponding fluid velocity components $\{u, v, w\}$. The fluid has density $\rho_{\rm av} + \rho_z z$. The imposed acceleration is of the form $\omega^2 A\{X''(\omega t), Y''(\omega t), Z''(\omega t) + G\}$, where $G$ is steady and $X''$, $Y''$, and $Z''$ are oscillatory. The oscillatory accelerations have period $2\pi/\omega$. $X''$, $Y''$, $Z''$, and $G$ are non-dimensional while $A$ has units of length. The primes indicate differentiation with respect to $\omega t$. The displacement vectors $X$, $Y$, and $Z$ each have zero mean, as do therefore the velocities $X'$, $Y'$, and $Z'$, and the accelerations. $A$ is defined by requiring the dimensionless displacement vector function $\{X, Y, Z\}$ or one of its dimensionless derivatives to have an amplitude of 1 in a suitable (chosen on a case-by-case basis) norm. $G$ and $\rho_z$ are both restricted to being positive. We thus consider only stable stratifications.

The imposed acceleration field together with the density gradient drive an oscillating shear flow. The momentum equations for the basic shear are

$$\frac{\partial \bar{u}}{\partial t} = \omega^2 A X''(\omega t) \frac{\rho_z}{\rho_{\rm av}} z, \tag{1}$$

$$\frac{\partial \bar{v}}{\partial t} = \omega^2 A Y''(\omega t) \frac{\rho_z}{\rho_{\rm av}} z, \tag{2}$$

with solutions

$$\bar{u} = \omega A X'(\omega t) \frac{\rho_z}{\rho_{\rm av}} z, \tag{3}$$

$$\bar{v} = \omega A Y'(\omega t) \frac{\rho_z}{\rho_{\rm av}} z. \tag{4}$$

The non-dimensionalized linearized equations for perturbations to this shear flow are

$$\frac{\partial u}{\partial x}+\frac{\partial v}{\partial y}+\frac{\partial w}{\partial z}=0, \tag{5a}$$

$$\frac{\partial u}{\partial t}+R\left(X'(t)\,z\frac{\partial u}{\partial x}+Y'(t)\,z\frac{\partial u}{\partial y}+X'(t)\,w\right)=-\frac{\partial p}{\partial x}+\nabla^2 u+X''(t)\,\rho, \tag{5b}$$

$$\frac{\partial v}{\partial t}+R\left(X'(t)\,z\frac{\partial v}{\partial x}+Y'(t)\,z\frac{\partial v}{\partial y}+Y'(t)\,w\right)=-\frac{\partial p}{\partial y}+\nabla^2 v+Y''(t)\,\rho, \tag{5c}$$

$$\frac{\partial w}{\partial t}+R\left(X'(t)\,z\frac{\partial w}{\partial x}+Y'(t)\,z\frac{\partial w}{\partial y}\right)=-\frac{\partial p}{\partial z}+\nabla^2 w+(Z''(t)+G)\,\rho, \tag{5d}$$

$$\frac{\partial \rho}{\partial t}+R\left(X'(t)\,z\frac{\partial \rho}{\partial x}+Y'(t)\,z\frac{\partial \rho}{\partial y}+w\right)=Pr^{-1}\nabla^2\rho. \tag{5e}$$

The same symbols have been kept for non-dimensional as for dimensional quantities. To obtain (5), the original dimensional equations are scaled by the viscous lengthscale $(\nu_{\mathrm{av}}/\omega)^{\frac{1}{2}}$, the timescale $1/\omega$, the velocity scale $\omega A$, the pressure scale $\omega^2 A\rho_{\mathrm{av}}(\nu_{\mathrm{av}}/\omega)^{\frac{1}{2}}$, and the density scale $\rho_{\mathrm{av}}$. $Pr$ is the Prandtl number $\nu_{\mathrm{av}}/\kappa_{\mathrm{av}}$, where $\kappa_{\mathrm{av}}$ is the average molecular or thermal diffusivity of the fluid. $R$ is equal to $A\rho_z/\rho_{\mathrm{av}}$.

Variants of (5) and of the scaling that was used to obtain it arise from two special cases. The first is when the fluid is both inviscid and non-diffusive. Then there is no lengthscale in the basic flow. The equations, however, retain the parameter $R$. The second is when the fluid is inviscid but has finite diffusivity. The appropriate lengthscale is then $(\kappa_{\mathrm{av}}/\omega)^{\frac{1}{2}}$ and $Pr^{-1}$ in (5*e*) is replaced by 1.

Equations (5*a–e*) have coefficients that are functions of both time and the vertical direction $z$. However, the coefficients' $z$ dependence can be eliminated by the transformation to Lagrangian coordinates

$$a=x-RX(t)\,z, \quad b=y-RY(t)\,z, \quad c=z. \tag{6}$$

This eliminates the $z$-dependent terms in (5) at the cost of complicating the $\partial/\partial z$ operator, which becomes

$$\frac{\partial}{\partial z}=\frac{\partial}{\partial c}-RX(t)\frac{\partial}{\partial a}-RY(t)\frac{\partial}{\partial b}. \tag{7}$$

The great advantage of the Lagrangian formulation is that the resulting $\{a,b,c\}$ independence of the coefficients allows the consideration of individual waves $\exp(\mathrm{i}(\alpha a+\beta b+\gamma c))$. The evolution of each wave is determined from the system of equations:

$$\alpha u+\beta v+(\gamma-\delta)\,w=0, \tag{8a}$$

$$\frac{\mathrm{d}u}{\mathrm{d}t}+l^2u=-\mathrm{i}\alpha p-RX'w+X''\rho, \tag{8b}$$

$$\frac{\mathrm{d}v}{\mathrm{d}t}+l^2v=-\mathrm{i}\beta p-RY'w+Y''\rho, \tag{8c}$$

$$\frac{\mathrm{d}w}{\mathrm{d}t}+l^2w=-\mathrm{i}(\gamma-\delta)\,p+(Z''+G)\,\rho, \tag{8d}$$

$$\frac{\mathrm{d}\rho}{\mathrm{d}t}+Pr^{-1}l^2\rho=-Rw, \tag{8e}$$

where $\delta = \alpha RX + \beta RY$ and $l^2 = \alpha^2 + \beta^2 + (\gamma - \delta)^2$. Application of the continuity equation (8$a$) to the momentum equations (8$b$–$d$) then reduces (8) to a system of two first-order ordinary differential equations:

$$\left(\frac{\mathrm{d}}{\mathrm{d}t} + l^2\right) l^2 w = ((\delta - \gamma)\alpha X'' + (\delta - \gamma)\beta Y'' + (\alpha^2 + \beta^2)(Z'' + G))\rho, \tag{9a}$$

$$\frac{\mathrm{d}\rho}{\mathrm{d}t} + Pr^{-1} l^2 \rho = -Rw. \tag{9b}$$

Equations (9$a$, $b$) are in a useful form as they stand. A second formulation, however, brings out additional aspects of the system dynamics: (9$a$, $b$) are first combined to yield a single second-order equation for $\rho$. The substitution

$$\rho = \frac{1}{(l^2)^{\frac{1}{2}}} \exp\left(-\frac{1}{2}\int^t (Pr^{-1} + 1)\, l^2 \,\mathrm{d}t\right)\tilde{\rho} \tag{10}$$

then gives

$$\frac{\mathrm{d}^2\tilde{\rho}}{\mathrm{d}t^2} + \left((Pr^{-1} - 1)\frac{\mathrm{d}l^2}{\mathrm{d}t} - \tfrac{1}{4}(Pr^{-1} - 1)^2 l^4 + \frac{(\alpha^2 + \beta^2)(Rl^2(Z'' + G) - (\mathrm{d}\delta/\mathrm{d}t)^2)}{l^4}\right)\tilde{\rho} = 0, \tag{11}$$

equation (11) is particularly useful for the case of large $R$.

We note briefly that the above approach can be extended to a fluid with an arbitrary number of chemical components so long as the gradients in composition are uniform. The gradient in composition fraction of each component can be oriented in any direction. Interesting and relatively simple cases that could be looked at include double-diffusive phenomena and situations in which the temperature and composition gradients are oriented perpendicularly to each other.

Before closing this section, we outline some of the basics of Floquet theory and nomenclature. The stability of solutions to (9) can be determined through its two linearly independent normal solutions. These are solutions in which $\{w(t+2\pi), \rho(t+2\pi)\} = \sigma\{w(t), \rho(t)\}$. We shall call the $\sigma$ Floquet factors. Instability is proved if one of the Floquet factors has a magnitude greater than one. The Floquet exponents $\lambda$ are defined in terms of the Floquet factors as $\exp(2\pi\lambda) = \sigma$. It can be shown that all unstable normal solutions of (9) have real $\sigma$ and thus the normal solutions are themselves real. This simplifies some stability proofs and results. Further information about the Floquet theory of second-order equations can be found in Stoker (1950).

## 3. Rayleigh–Taylor case

The coefficients of (9) depend on three non-dimensional parameters, on the disturbance wavenumber, and on a very general vector function. Rather than consider (9) in all this generality, we shall attempt to gain an idea of the range of instability dynamics by examining some particular cases. We begin by briefly considering instabilities of Rayleigh–Taylor type. These will be shown to provide a considerable contrast to Kelvin–Helmholtz instabilities, which will be considered in detail in §§4 and 5.

In the Rayleigh–Taylor case the accelerations are parallel to the density gradient and thus the basic state is motionless. With no motion, $\delta$ is zero and $l^2$ is constant. Equation (11) becomes

$$\frac{\mathrm{d}^2\tilde{\rho}}{\mathrm{d}t^2} + \left(-\tfrac{1}{4}(Pr^{-1} - 1)^2 l^4 + \frac{\alpha^2 + \beta^2}{l^2} R(Z'' + G)\right)\tilde{\rho} = 0, \tag{12}$$

with $l^2 = \alpha^2+\beta^2+\gamma^2$. This has closed-form solutions for $Z''$ made up of impulses, being piecewise constant, and being continuous and piecewise linear. Also, when $Z'' = \cos t$, (12) becomes Mathieu's equation, solutions of which are discussed in detail by Arscott (1964).

We shall discuss three aspects of the general behaviour of Rayleigh–Taylor instabilities. First, a Squires theorem can be proved. From (10) and (12), the Floquet exponents of the system are dependent on four parameters: $l^2$, $Pr$, $G$, and $\check{R} = (\alpha^2+\beta^2/l^2)R$. From the relationship between $R$ and $\check{R}$, the minimum $R$ that produces a given growth rate is equal to the minimum $\check{R}$ and occurs when $\gamma = 0$. In particular, the critical $R$ is thus found for $\gamma = 0$.

Next, we consider the onset of instability when $G = 0$ (or is small enough to be neglected). Non-zero lower bounds on the critical $R$ can then be proved for all integrable $Z''$. The proof, which will only be outlined here, is in two steps. Equations (9*a*, *b*) can be combined to yield

$$\left(\frac{\mathrm{d}}{\mathrm{d}t}+l^2\right)\left(\frac{\mathrm{d}}{\mathrm{d}t}+Pr^{-1}l^2\right)\rho+\frac{\alpha^2+\beta^2}{l^2}RZ''\rho = 0. \tag{13}$$

In the first step of the proof it is shown that any unstable normal solution of (13) must have at least one zero in every interval of length $2\pi$. The second step, based on a proof by Lyapunov (Bellman 1953, pp. 123–125), shows from equation (12) that this is impossible unless

$$\int_0^{2\pi} \check{R}|Z''|\,\mathrm{d}t \geqslant \frac{2}{\pi}.$$

Thus,
$$\check{R}_{\mathrm{crit}} \geqslant \frac{2}{\pi}\Big/\int_0^{2\pi} |Z''|\,\mathrm{d}t.$$

This bound is found for the case $l^2 = 0$, which is the value of $l^2$ that makes solutions to (12) most rapidly oscillatory. A lower bound on unstable $\check{R}$ can be found as a function of $l^2$ from (12) using non-oscillation theorems of Moore (1956). This lower bound increases monotonically with increasing $l^2$.

Lastly, we note the dependence of the Floquet exponent on $R$ as $R$ becomes large. For $G$ zero or dominated by $Z''$, a quasi-steady analysis of (12) gives $\lambda = O(R^{\frac{1}{2}})$.

## 4. Kelvin–Helmholtz case, $G = 0$

We now consider the case of accelerations perpendicular to the density gradient. This section considers the case $G = 0$. The effect of $G$ will be considered in §5. For simplicity, we set $Y = Z = 0$ and $\beta = 0$ throughout this section.

The oscillating base-state velocity field of the Kelvin–Helmholtz case greatly affects the stability characteristics of the system. First, unlike the Rayleigh–Taylor case, the critical $R$ of any forcing is zero. This can be seen through an examination of equations (10) and (11). As the wavenumber vector $\{\alpha, \gamma\}$ goes to zero these reduce to

$$\rho = \frac{1}{(l^2)^{\frac{1}{2}}}\tilde{\rho}, \quad \frac{\mathrm{d}^2\tilde{\rho}}{\mathrm{d}t^2} - \frac{R^2(X')^2}{\left(\left(RX-\dfrac{\gamma}{\alpha}\right)^2+1\right)^2}\tilde{\rho} = 0. \tag{14}$$

For $R > 0$, the coefficient of $\tilde{\rho}$ is less than or equal to 0 for all $t$ and $\tilde{\rho}$ increases exponentially. $\rho$ oscillates but its Floquet exponent is the same as that of $\tilde{\rho}$. In the

limit $R \to 0$, $\tilde{\rho}$ grows linearly in $t$. The most significant difference, however, between the Kelvin–Helmholtz and the Rayleigh–Taylor instabilities occurs at high $R$. The effect of the Kelvin–Helmholtz shear is to change the effective vertical wavenumber from $\gamma$ to $\gamma - \alpha RX$. Unless $\alpha$ is very small, a large $R$ results at most times in a large $l^2$. From (9$a$), large $l^2$ has the effect of suppressing $w$, and, from (9$b$), this suppresses the creation of additional $\rho$. The result, as will be shown, is a very weak increase in maximum instability growth rate with increasing $R$. Thus, though Kelvin–Helmholtz instability dominates at small $R$, Rayleigh–Taylor instability will be found to be most important at moderate and large $R$. The above argument holds for both the non-diffusive and diffusive cases. In the latter case it can also happen that an increase in $R$ can directly stabilize a wave by increasing the amount of viscous and molecular diffusive damping.

The case $Pr = 1$ is a bit simpler than general $Pr$ because a transformation can be applied that separates out diffusive effects. Most of §4 will therefore be limited to this case. However, only general features that are applicable for general $Pr$ will be emphasized. Additional phenomena that occur for other values of $Pr$ will be considered briefly in §4.4.

### 4.1. *Overview, $Pr = 1$*

For $Pr = 1$, and with $Y(t) = Z(t) = \beta = 0$, equations (9$a$, $b$) become

$$\left(\frac{\mathrm{d}}{\mathrm{d}t} + l^2\right) l^2 w = (\alpha RX - \gamma)\, \alpha X'' \rho, \tag{15a}$$

$$\frac{\mathrm{d}\rho}{\mathrm{d}t} + l^2 \rho = -Rw. \tag{15b}$$

The transformations

$$\rho = R \exp\left(-\int^t l^2 \,\mathrm{d}t\right) \hat{\rho}, \quad w = \exp\left(-\int^t l^2 \,\mathrm{d}t\right) \hat{w} \tag{16}$$

and the substitutions

$$\tilde{X} = X - \frac{\gamma}{\alpha R}, \quad \epsilon = R^{-1} \tag{17}$$

reduce (15) to the simple form

$$\frac{\mathrm{d}}{\mathrm{d}t}(\tilde{X}^2 + \epsilon^2)\, \hat{w} = \tilde{X}\tilde{X}'' \hat{\rho}, \tag{18a}$$

$$\frac{\mathrm{d}\hat{\rho}}{\mathrm{d}t} = -\hat{w}. \tag{18b}$$

The effect of the transformations (16) is to separate out diffusive effects from the equation. Alternatively, (18) can be seen as the viscous case in the long-wave limit $\alpha \to 0$, $\gamma \to 0$ with $\gamma/\alpha R$ zero or finite.

This section demonstrates some of the chief features of the Kelvin–Helmholtz case by showing results of numerical calculations for $X = \cos t$. Analytical solutions that further illustrate these features will be developed in following sections. In this section, results will primarily be given for the diffusive equations (15). The exception is results given in figure 5, which are from (18). The analysis in §§4.2 and 4.3 will use (18).

We first consider the variation of the Floquet exponent $\lambda$ with wavenumber. Figure 1 shows the Floquet exponents as a function of $\gamma/\alpha R$ for $\alpha R = 0.5$ and 1.0, for

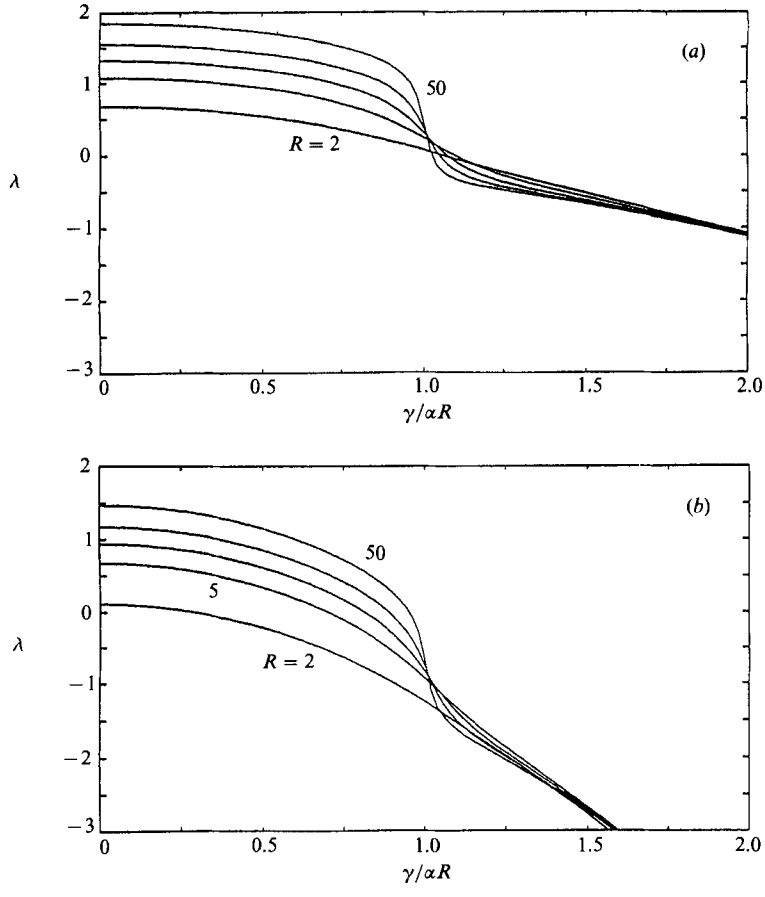


FIGURE 1. $\lambda$ as a function of $\gamma/\alpha R$ for $R = 2$, 5, 10, 20, and 50; $X = \cos t$. (*a*) $\alpha R = 0.5$, (*b*) $\alpha R = 1.0$.

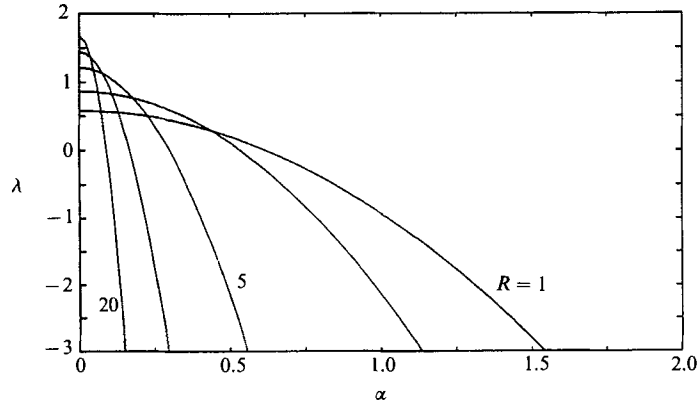


FIGURE 2. $\lambda$ as a function of $\alpha$ for $\gamma = 0$, for $R = 1$, 2, 5, 10, and 20; $X = \cos t$.

$R = 2$, 5, 10, 20, and 50. The results show that $\lambda$ is a monotonically decreasing function of $\gamma$. (For $Pr = 1$, $\lambda$ is always real and it is usually real for general $Pr$.) Near $\gamma = 0$ this decrease is very gradual. At the larger values of $R$ there is a sharp decrease in $\lambda$ as $\gamma/\alpha R$ goes through 1. This, as will be shown in detail, is associated with the

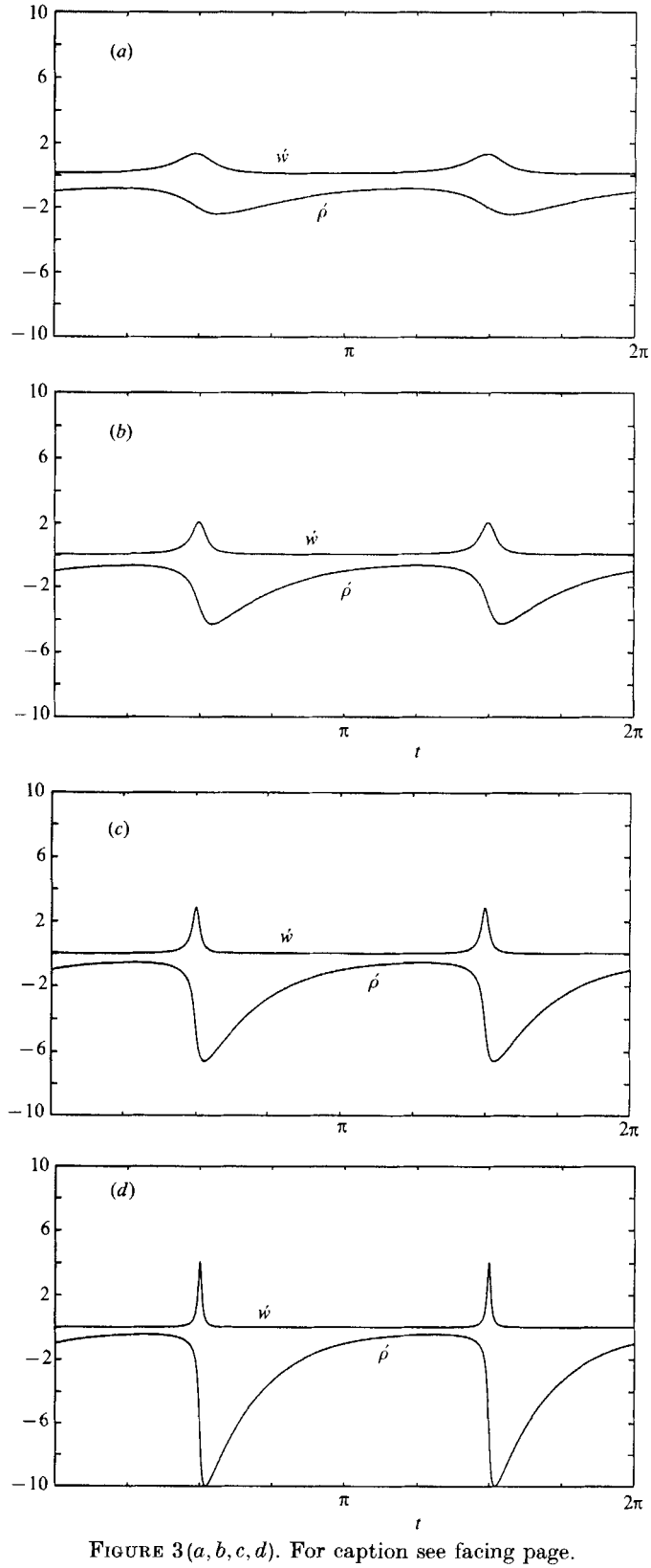


FIGURE 3(a, b, c, d). For caption see facing page.

disappearance of 'zero points'. These are times when the effective vertical wavenumber $\gamma - \alpha RX$ is zero. Wave growth is most rapid at these times. As $\gamma/\alpha R$ becomes large $\lambda$ becomes linear in $\gamma$ and approximately independent of $R$.

Figure 2 shows $\lambda$ as a function of $\alpha$ for $\gamma = 0$ and $R = 1, 2, 5, 10$, and 20. This shows that as $R$ increases the range of unstable $\alpha$ decreases, the range being roughly $O(1/R)$. This occurs even though the maximum $\lambda$ increases with $R$. The trend is also hinted at in figure 1.

Figures 3 and 4 show the behaviour of normal solutions for different $R$ and $\gamma/\alpha R$. The purpose of the figures is to show the importance of the zero points in the instability process. At large $R$, growth of the instability wave is concentrated in small regions about these points. The figures show $\acute{\rho}$ and $\acute{w}$, where $\{\rho, w\} = \{\acute{\rho}, \acute{w}\} \exp(\lambda t)$. $\acute{\rho}$ and $\acute{w}$ are periodic with period $2\pi$ (Stoker 1950). In the figures, $\acute{\rho}$ is always negative while $\acute{w}$ is positive.

Figure 3 gives the unstable normal solutions for $\gamma = 0$, $\alpha R = 0.5$, for $R = 4$, 10, 20, and 40. The zero points are at $\frac{1}{2}\pi$ and $\frac{3}{2}\pi$. Even at $R = 4$ wave growth is concentrated near the zero points. $\acute{w}$ shows a pronounced peak at zero points and $\acute{\rho}$, driven by $\acute{w}$, increases rapidly in amplitude. As $R$ increases, the peaks in $\acute{w}$ become increasingly sharp, their widths being $O(1/R)$. Away from these peaks $\acute{w}$ is nearly zero and $\acute{\rho}$ decreases monotonically in amplitude. This decrease also occurs for $\rho$ itself.

Figure 4 shows normal solutions for $R = 40$, $\alpha R = 0.5$, for $\gamma = 0.44$, 0.47, 0.5, and 0.53. The figure shows how the normal solution changes as zero points disappear. At $\gamma = 0.5$ there is only one zero point, at $t = 0$, per period and at $\gamma = 0.53$ there are none. As $\gamma$ approaches 0.5, the $\acute{w}$ and $\acute{\rho}$ peaks diminish and become smoother. The smoothing is due to the decrease in $X'$ at the zero point as $\gamma/\alpha R$ increases; the zero-point region has thickness that varies inversely with $X'$. The lowered peaks are due to the somewhat paradoxical fact that the slower the base flow moves through a zero point the less the instability growth. This is derived analytically (equations (32), (33)) in §4.3. The peaks in $\acute{w}$ essentially disappear for $\gamma = 0.5$ and 0.53. The wave is still unstable at $\gamma = 0.5$, where $\lambda = 0.438$, but is stable at $\gamma = 0.53$, where $\lambda = -0.186$. The wave grows in amplitude in the vicinity of $\cos t = 1$ even for $\gamma = 0.53$ but this growth is more than offset by the steady decay of the wave at all other times.

Figure 5 gives another look at the effect of zero points. Results are from equation (18). The figure shows $\log \hat{\sigma}$, the unstable Floquet factor for (18), plotted against $\log R$ for values of $\gamma/\alpha R$ near 1. For small $R$ a rapid increase in $\hat{\sigma}$ is shown for all $\gamma/\alpha R$ but for large $R$ the $\log \hat{\sigma}$ curves separate out according to whether $\gamma/\alpha R$ is less than, equal to, or greater than one. For $\gamma/\alpha R > 1$ (no zero points) the curves eventually return to 0. For $\gamma/\alpha R = 1$ (one zero point) the curve asymptotes to a slope of roughly $\frac{1}{2}$ ($\hat{\sigma} \approx O(R^{\frac{1}{2}})$). For $\gamma/\alpha R < 1$ the curves asymptote to a slope of 2 ($\hat{\sigma} = O(R^2)$).

### 4.2. *Solution for impulse accelerations, Pr = 1*

Closed-form solutions of (18) can be derived for the case of flow driven by impulse (delta-function) accelerations. An impulse acceleration model provides a useful approximation to a given base flow provided that the impulse model's $X$ and $X'$ are equal to the original flow's $X$ and $X'$ at the original flow's zero points. It turns out, as will be shown in §4.3, that the exact form of $X''$ itself is relatively unimportant.

---

FIGURE 3. Periodic components $\acute{w}$ and $\acute{\rho}$ of the unstable normal solutions for $\gamma = 0$, $\alpha R = 0.5$, for (*a*) $R = 4$, (*b*) 10, (*c*) 20, and (*d*) 40; $X = \cos t$. In the figures, $\acute{w}$ is always positive while $\acute{\rho}$ is negative. The Floquet exponents of the solutions are (*a*) 0.99, (*b*) 1.32, (*c*) 1.55, and (*d*) 1.78.

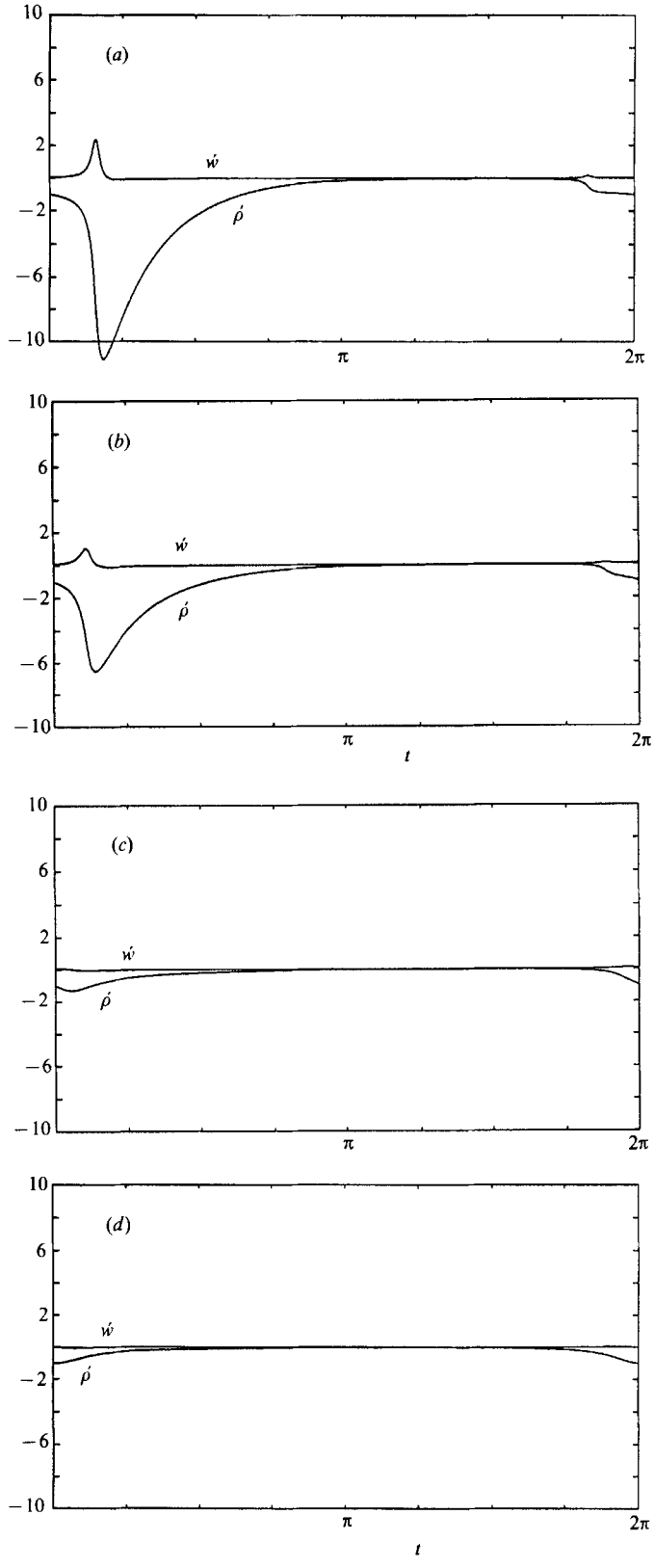


FIGURE 4(a, b, c, d). For caption see facing page.

In this section we shall briefly develop the solution for the impulse model and then apply it to look at bounds on unstable wavenumbers and to look at the role of zero points.

Solution for impulse forcings is straightforward. From (18), between impulses $\hat{w} = C/(\tilde{X}^2+\epsilon^2)$, where $C$ is a constant. From this, $\hat{w}$ has a spike in amplitude at zero points. $\hat{w}/C$ is then $O(R^2)$ while away from zero points $\hat{w}/C$ is $O(1)$. From (18*b*) $\hat{\rho}$ varies according to $\tan^{-1} R\tilde{X}$. The bulk of change in $\hat{\rho}$ thus occurs in an $O(\epsilon/\tilde{X}')$ wide region about each zero point.

Transition formulae can be derived that relate solutions for $\hat{w}$ and $\hat{\rho}$ across impulse points, and from this general expressions for the $\hat{\sigma}$, the Floquet factors of (18), can be derived. However, this general result is not particularly illuminating. Instead, we jump to consideration of a particular case, two impulses per time period, of strengths $\pm I, I$ positive, the first at $t = 0$ and the second at $t = \pi$. The resulting Floquet factor is

$$\hat{\sigma} = \Lambda \pm (\Lambda^2-1)^{\frac{1}{2}}, \tag{19a}$$

where

$$\Lambda = 1+\pi IR\Psi-2\tilde{X}_{\max}\tilde{X}_{\min}R^2\Psi^2 \tag{19b}$$

and

$$\tilde{X}_{\max} = \tfrac{1}{4}\pi I-\frac{\gamma}{\alpha R}, \quad \tilde{X}_{\min} = -\tfrac{1}{4}\pi I-\frac{\gamma}{\alpha R}, \quad \Psi = \tan^{-1}(R\tilde{X}_{\max})-\tan^{-1}(R\tilde{X}_{\min}). \tag{19c}$$

The Floquet factors for the original variables $\rho$ and $u$ are

$$\sigma = \exp(-\tfrac{1}{24}\pi^3 I^2\alpha^2R^2)\exp(-2\pi(\alpha^2+\gamma^2))\,\hat{\sigma}. \tag{20}$$

Perhaps the most significant result from (19) and (20) is the very weak increase of growth rate, relative to the Rayleigh–Taylor case, with increasing $R$. This is due to the enhanced diffusive and shear-related damping that occurs at large $R$. The Floquet exponent of the fastest growing wave increases only as $O(\ln R)$. Further, this increase is sustained as $R\to\infty$ only for $\alpha\to 0$. For any finite, fixed $\alpha$ viscous effects enforce stability at large enough $R$. Then, $\lambda\to O(-\alpha^2R^2)$.

The effect of zero points is seen in (19) through $\Psi$. With two zero points, as $R\to\infty$, $\Psi\to\pi$. Then $\Lambda\to O(R^2)$. With one zero point (either $\tilde{X}_{\max}$ or $\tilde{X}_{\min}$ equal to zero) $\Psi\to\frac{1}{2}\pi$ and $\Lambda\to O(R)$. With no zero points $\Lambda\to 1$. The first and last results are in agreement with the results of figure 5 for $X = \cos t$. The one-zero-point result is different,with the sinusoidal $\hat{\sigma}$ being roughly $O(R^{\frac{1}{2}})$ rather than $O(R)$. This difference is probably due to the occurrence in the impulse case of an impulse right at the zero point.

Useful upper bounds on unstable wavenumbers can also be determined. These bounds hold approximately for sinusoidal and other types of accelerations. Results confirm what was observed in §4.1. From (19) and (20) the largest unstable $|\alpha|$ occurs when $\gamma = 0$. Then

$$\alpha^2 = \frac{\ln(\hat{\sigma}(R,\gamma=0))}{\frac{1}{24}\pi^3I^2R^2+2\pi}. \tag{21}$$

At large $R$, $\hat{\sigma}$ is close to but bounded below $2\Lambda$. This can be used to derive the approximate upper bound

$$\alpha^2 \leqslant \frac{\ln(\frac{1}{4}\pi^4I^2R^2+2\pi^2IR+2)}{\frac{1}{24}\pi^3I^2R^2+2\pi}. \tag{22}$$

FIGURE 4. Periodic components $\hat{w}$ and $\hat{\rho}$ of normal solutions for $R = 40$, $\alpha R = 0.5$, for (*a*) $\gamma = 0.44$, (*b*) 0.47, (*c*) 0.50, and (*d*) 0.53; $X = \cos t$. In the figures, $\hat{w}$ is always positive while $\hat{\rho}$ is negative. The Floquet exponents of the solutions are (*a*) 1.23, (*b*) 1.04, (*c*) 0.44, and (*d*) −0.19.

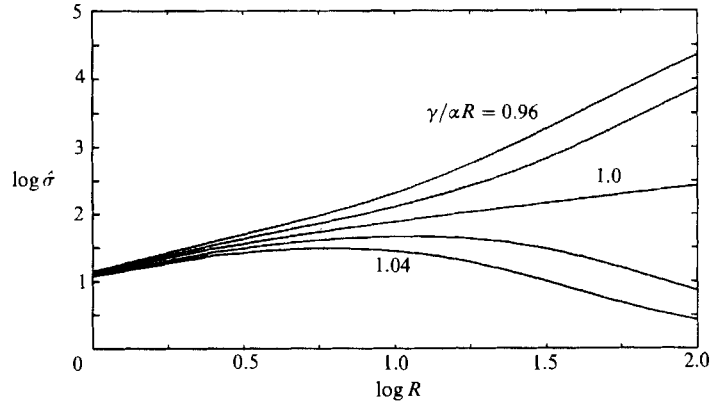


FIGURE 5. $\log\hat{\sigma}$ as a function of $\log R$, for $\gamma/\alpha R = 0.96$, 0.98, 1.00, 1.02, and 1.04; $X = \cos t$.

An upper bound on unstable $\gamma^2$ can be found in a similar manner. It is

$$\gamma^2 \leqslant \frac{\ln(\frac{1}{4}\pi^4 I^2 R^2 + 2\pi^2 IR + 2)}{2\pi}. \tag{23}$$

Roughly, the maximum unstable $|\alpha|$ is $O(\ln R/R)$, while the maximum unstable $|\gamma|$ is $O(\ln R)$.

It should be remembered that the system was non-dimensionalized using the Stokes viscous lengthscale. The limit on the unstable effective vertical wavenumber $\gamma - \alpha RX(t)$ of $O(\ln R)$ is thus consistent with the expected dominance of viscous damping at the Stokes scale. Since the Stokes scale is often quite small, the modest looking limits on $\gamma$ and $\alpha R$ in fact indicate the possible existence of very short-wavelength instabilities.

### 4.3. *Asymptotic solutions for Pr = 1 and large R*

Both the numerics of §4.1 and the impulse solution of §4.2 have shown the importance of zero points. As $R \to \infty$ these points are in fact necessary for instability. Significant wave growth is then limited to narrow regions surrounding these points. Away from zero points $w$ is comparatively quite small and $\rho$ is relatively quiescent. In this section, we show how to construct a matched asymptotic solution, valid at large $R$ for general forcing, that takes advantage of these phenomena. It turns out that it is possible to construct a general solution to (18) that has a relative error of $O(\epsilon^2 \ln R)$ and that yields matching formulae that depend only on the local behaviour of $X$ at zero points.

From (18), the second-order equation for $\hat{\rho}$ is

$$\frac{\mathrm{d}}{\mathrm{d}t}(\tilde{X}^2 + \epsilon^2)\frac{\mathrm{d}\hat{\rho}}{\mathrm{d}t} + \tilde{X}\tilde{X}''\hat{\rho} = 0. \tag{24}$$

For away from zero points, (24) is most usefully rearranged to

$$\frac{\mathrm{d}^2}{\mathrm{d}t^2}(\tilde{X}\hat{\rho}) = -\frac{\epsilon^2}{\tilde{X}}\frac{\mathrm{d}^2\hat{\rho}}{\mathrm{d}t^2}. \tag{25}$$

For near the $n$th zero point $t = t_n$ we expand $\tilde{X}$ in a Taylor series in $t - t_n$,

$$\tilde{X} = \tilde{X}_n'(t-t_n) + \tfrac{1}{2}\tilde{X}_n''(t-t_n)^2 + \ldots.$$

Substitution of the 'fast' variable $T = (t-t_n)/\epsilon$ into (24) then yields

$$\frac{\mathrm{d}}{\mathrm{d}T}(\tilde{X}_n'^2 T^2+1)\frac{\mathrm{d}\hat{\rho}}{\mathrm{d}T} = -\epsilon\left(\tilde{X}_n'\tilde{X}_n'' T+\frac{\mathrm{d}}{\mathrm{d}t}\tilde{X}_n'\tilde{X}_n'' T^3\right)+O(\epsilon^2). \tag{26}$$

The process of constructing solutions proceeds as follows. The outer solutions in $t-t_n<0$ are denoted by $\hat{\rho}_1^{n,-}$ and $\hat{\rho}_2^{n,-}$. These must be connected to the outer solutions in $t-t_n>0$, $\hat{\rho}_1^{n,+}$ and $\hat{\rho}_2^{n,+}$, using inner solutions $\hat{\rho}_1^{n,\mathrm{i}}$ and $\hat{\rho}_2^{n,\mathrm{i}}$. The outer solutions in $t-t_n>0$ must then be connected to the outer solutions in $t-t_{n+1}<0$ for the next zero point. The goal is to find $C_1^{n+1,-}\hat{\rho}_1^{n+1,-}+C_2^{n+1,-}\hat{\rho}_2^{n+1,-}$ given $C_1^{n,-}\hat{\rho}_1^{n,-}+C_2^{n,-}\hat{\rho}_2^{n,-}$.

The outer solutions are

$$\hat{\rho}_1^{n,\pm} = \frac{\tilde{X}_n'}{\tilde{X}}(t-t_n)+O(\epsilon^2\ln R), \quad \hat{\rho}_2^{n,\pm} = \frac{\tilde{X}_n'}{\tilde{X}}+\frac{1}{2}\frac{\tilde{X}_n''}{\tilde{X}}(t-t_n)+O(\epsilon^2\ln R). \tag{27}$$

The transition formulae giving $C_1^{n+1,-}$ and $C_2^{n+1,-}$ from $C_1^{n,+}$ and $C_2^{n,+}$ are

$$C_1^{n+1,-} = \frac{\tilde{X}_n'}{\tilde{X}_{n+1}'}\left(1-\tfrac{1}{2}(t_{n+1}-t_n)\frac{\tilde{X}_{n+1}''}{\tilde{X}_{n+1}'}\right)C_1^{n,+}+ \\ +\frac{1}{2}\left(\frac{\tilde{X}_n''}{\tilde{X}_{n+1}'}-\frac{\tilde{X}_n'\tilde{X}_{n+1}''}{\tilde{X}_{n+1}'^2}-\tfrac{1}{2}(t_{n+1}-t_n)\frac{\tilde{X}_n''\tilde{X}_{n+1}''}{\tilde{X}_{n+1}'^2}\right)C_2^{n,+}, \tag{28a}$$

$$C_2^{n+1,-} = (t_{n+1}-t_n)\frac{\tilde{X}_n'}{\tilde{X}_{n+1}'}C_1^{n,+}+\left(\frac{\tilde{X}_n'}{\tilde{X}_{n+1}'}+\tfrac{1}{2}(t_{n+1}-t_n)\frac{\tilde{X}_n''}{\tilde{X}_{n+1}'}\right)C_2^{n,+}. \tag{28b}$$

These formulae have a relative error of $O(\epsilon^2\ln R)$. They can be derived by comparing the coefficients of $t^0$ and $t^1$ in the numerators in equation (27).

As $t-t_n\to 0$

$$\hat{\rho}_1^{n,\pm}\to 1-\tfrac{1}{2}\epsilon\frac{\tilde{X}_n''}{\tilde{X}_n'}T+O(\epsilon^2\ln R), \quad \hat{\rho}_2^{n,\pm}\to\epsilon^{-1}(T^{-1}+O(\epsilon^2\ln R)). \tag{29}$$

The inner solutions that match to the outer solutions as $T\to-\infty$ are

$$\hat{\rho}_1^{n,\mathrm{i}} = 1-\frac{\epsilon}{2}\frac{\tilde{X}_n''}{\tilde{X}_n'}T+O(\epsilon^2\ln R), \tag{30a}$$

$$\hat{\rho}_2^{n,\mathrm{i}} = -\epsilon^{-1}(\tilde{X}_n'\tan^{-1}(\tilde{X}_n'T)+|\tilde{X}_n'|\tfrac{1}{2}\pi) \\ +\frac{1}{2}\frac{\tilde{X}_n''}{\tilde{X}_n'}\left(\frac{1}{\tilde{X}_n'^2T^2+1}+\tilde{X}_n'T\tan^{-1}(\tilde{X}_n'T)+1+\tfrac{1}{2}\pi|\tilde{X}_n'|T\right)+O(\epsilon\ln R), \tag{30b}$$

As $T\to+\infty$

$$\hat{\rho}_1^{n,\mathrm{i}}\to 1-\tfrac{1}{2}\epsilon\frac{\tilde{X}_n''}{\tilde{X}_n'}T+O(\epsilon^2\ln R), \tag{31a}$$

$$\hat{\rho}_2^{n,\mathrm{i}}\to-\epsilon^{-1}\pi|\tilde{X}_n'|\left(1-\frac{\epsilon}{2}\frac{\tilde{X}_n''}{\tilde{X}_n'}T\right)+\epsilon^{-1}\frac{1}{T}+O(\epsilon\ln R), \tag{31b}$$

from which

$$\hat{\rho}_1^{n,-}\to\hat{\rho}_1^{n,+}+O(\epsilon^2\ln R), \tag{32a}$$

$$\hat{\rho}_2^{n,-}\to-\epsilon^{-1}|\tilde{X}_n'|\pi\hat{\rho}_1^{n,+}+\hat{\rho}_2^{n,+}+O(\epsilon\ln R). \tag{32b}$$

Alternatively, given $C_1^{n,-}\hat{\rho}_1^{n,-}+C_2^{n,-}\hat{\rho}_2^{n,-}$, then

$$C_1^{n,+} = C_1^{n,-}-\epsilon^{-1}|\tilde{X}_n'|\pi C_2^{n,-}, \quad C_2^{n,+} = C_2^{n,-}. \tag{33}$$

Equation (33) has a relative error of $O(\epsilon^2 \ln R)$. The combination of (28) and (33) gives the overall transition from $C_1^{n,-}\hat{\rho}_1^{n,-}+C_2^{n,-}\hat{\rho}_2^{n,-}$ to $C_1^{n+1,-}\hat{\rho}_1^{n+1,-}+C_2^{n+1,-}\hat{\rho}_2^{n+1,-}$.

The above results have brought out several general features of the instability process. Equations (32) and (33) show that at zero points the growth of the instability is extremely rapid, with growth $O(|X_n'|\pi R)$. In contrast, (27) shows that away from zero points $\tilde{X}\hat{\rho}$ is nearly linear and thus that $\hat{\rho}$ is then essentially neutral. Equations (27) and (28) also verify that the acceleration does not directly affect the overall stability process. The acceleration's significance is merely that it forces a return to zero points. How it accomplishes this is not of particular importance. The transition formulae (28) and (33) are both dependent only on the local behaviour of $X$ near zero points, so all $X''$ that produce that behaviour, whether, for example, step functions or sinusoidal, will produce essentially the same rate of instability. Wave behaviour at a zero point is only very weakly (a relative effect of $O(\epsilon^2 \ln R)$) affected by second- and higher-order derivatives of $X$. That is why instability evolution can be usefully approximated by an impulse model. Higher-order derivatives of $X$ are most important in the transition formulae for between zero points. In them, however, they still have a relative effect of only $O(\epsilon)$.

The matching formulae (28) and (33) can be simplified to give a bare-bones but clearer picture of the overall instability process. $C_1^{n,-}$ and $C_2^{n,-}$ are generally of comparable amplitude. However, $C_2^{n,-}$ is of greater importance because it is the factor that gets amplified. Once through the zero point $\hat{\rho}_1^{n,+}$ dominates, $C_1^{n,+}$, being $O(R)$ times greater than $C_2^{n,+}$. In the transition to the region $t < t_{n+1}$ this inequality is eliminated. Once again, $C_2$ is most important in determining the instability evolution. The overall process can be reduced to

$$C_1^{n,+} \approx -\pi|\tilde{X}_n'|RC_2^{n,-}, \quad C_2^{n+1,-} \approx (t_{n+1}-t_n)\frac{\tilde{X}_n'}{\tilde{X}_{n+1}'}C_1^{n,+}. \tag{34}$$

Thus,
$$C_2^{n+1,-} \approx \pi(t_{n+1}-t_n)\,|\tilde{X}_n'|\left|\frac{\tilde{X}_n'}{\tilde{X}_{n+1}'}\right|RC_2^{n,-}. \tag{35}$$

With two zero points per period, the Floquet factor $\hat{\sigma}$ is, approximately

$$\hat{\sigma} \approx \pi^2(t_2-t_1)\,(2\pi+t_1-t_2)\,|\tilde{X}_1'|\,|\tilde{X}_2'|R^2. \tag{36}$$

We note that for the two-delta-function case

$$t_2-t_1 = \pi-\frac{4}{I}\frac{\gamma}{\alpha R} \quad \text{and} \quad |\tilde{X}_1'| = |\tilde{X}_2'| = \tfrac{1}{2}I.$$

Equation (36) for this case becomes $-4\tilde{X}_{\max}\tilde{X}_{\min}\pi^2R^2$. It thus reproduces the dominant term in (19$a$, $b$).

Table 1 gives results for $\tilde{X} = \cos t - 0.5$ from (28), (33) and from the simpler formula (36). The approximate $\hat{\sigma}$ from both approximations is compared to the exact $\hat{\sigma}$. The results show that, as a practical matter, both approximations are adequately accurate down to $R$ of about 6. The absolute error in the second-order approximation is, as expected, nearly independent of $R$. The absolute error from (36) is $O(R)$, giving a relative error of $O(\epsilon)$.

### 4.4. *Notes on when* $Pr \neq 1$

In most respects, wave behaviour with $Pr \neq 1$ is qualitatively the same as for $Pr = 1$. We briefly discuss two areas of difference. The first is the range of unstable $\alpha$, which was found to be very limited when $Pr = 1$. In contrast, when $Pr = 0$,

| $R$ | $\hat{\sigma}_{\text{exact}}$ | $\hat{\sigma}_{\epsilon^2}$ | $\hat{\sigma}_{\epsilon^1}$ |
|---|---|---|---|
| 2 | 142 | 193 | 260 |
| 4 | 753 | 904 | 1039 |
| 6 | 1909 | 2134 | 2338 |
| 8 | 3604 | 3884 | 4156 |
| 10 | 5831 | 6154 | 6494 |
| 20 | 24841 | 25294 | 25976 |
| 30 | 56895 | 57422 | 58455 |
| 40 | 101959 | 102538 | 103903 |
| 50 | 160023 | 160641 | 162349 |
| 60 | 231083 | 231733 | 233782 |
| 80 | 412178 | 412879 | 415613 |
| 100 | 645237 | 645978 | 649395 |

TABLE 1. Exact and approximate $\hat{\sigma}(R)$ for $\tilde{X} = \cos t - 0.5$. The second column gives the exact $\hat{\sigma}$, the third the $O(\epsilon^2 \ln R)$-accurate $\hat{\sigma}$ from equations (28), (33), and the fourth gives the $O(\epsilon)$-accurate $\hat{\sigma}$ from equation (36)

$\alpha$ can be in the unstable range even as it becomes infinite. With $Pr = 0$ and with, as before, $Y'' = Z'' = \beta = 0$, (9) becomes

$$\left(\frac{\mathrm{d}}{\mathrm{d}t} + l^2\right) l^2 w = (\delta - \gamma)\,\alpha X'' \rho, \tag{37a}$$

$$\frac{\mathrm{d}\rho}{\mathrm{d}t} = -Rw. \tag{37b}$$

Instability can be proved if $(\delta - \gamma)\,\alpha X''$ is always negative. When that holds, if $\rho$ and $w$ are of opposite sign they remain of opposite sign. But then, from (37*b*), $|\rho|$ must increase monotonically. $(\delta - \gamma)\,\alpha X''$ always negative holds as $\alpha \to \infty$, for example for the model two-delta-function case examined in §4.2 and for sinusoidal forcing with $\gamma = 0$. The same result also holds for the case $Pr = \infty$ (with lengthscale then being $(\kappa/\omega)^{\frac{1}{2}}$).

The second difference is the possible occurrence of subharmonic solutions. Equation (11) can be used to prove that when $Pr = 1$ normal solutions for $\rho$ are necessarily harmonic. Then the coefficient of $\tilde{\rho}$ is necessarily negative and normal solutions for $\tilde{\rho}$ are monotonic. The Floquet factor thus has to be positive and the Floquet exponent real. However, when $Pr \neq 1$ the term $(Pr^{-1} - 1)\,\mathrm{d}l^2/\mathrm{d}t$ in (11) can make $\tilde{\rho}$ oscillatory. This occurs over a single intermediate range of $l^2$, since for $l^2$ too small $-(\mathrm{d}\delta/\mathrm{d}t)^2/l^4$ dominates and for $l^2$ large $-\frac{1}{4}(Pr^{-1} - 1)^2 l^4$ dominates.

## 5. Kelvin–Helmholtz case, non-zero $G$

We now consider the Kelvin–Helmholtz case as modified by a positive (statically stable) $G$. To simplify matters, consideration is limited to $Pr = 1$, $Y(t) = Z(t) = \beta = 0$. Analytic solutions will be discussed for impulse forcing. As with $G = 0$ these solutions give some useful qualitative results. Also, we shall show numerical solutions for $X = \cos t$.

The most useful parameter with which to discuss results is not $G$ itself but rather $G/R\tilde{X}'^2$. This is the flow's local (in time) Richardson number. In terms of the original dimensional quantities, $Ri$ is $(\rho_z \omega^2 AG)/(\rho_{\text{av}}\, \bar{u}_z^2)$; $\omega^2 AG$ is the dimensional steady acceleration. It is well known (Howard 1961) that for steady, inviscid, parallel flows

$Ri(z)$ everywhere greater than $\frac{1}{4}$ is sufficient for stability. For the unsteady case considered here, this sufficiency will be shown to be a practical but no longer exact guide. $Ri = \frac{1}{4}$ becomes the approximate boundary between strong and weak instabilities rather than the instability cutoff.

With $Pr = 1$, and with $Y(t) = Z(t) = \beta = 0$, equations (9$a$, $b$) are

$$\left(\frac{\mathrm{d}}{\mathrm{d}t} + l^2\right) l^2 w = ((\alpha RX - \gamma)\,\alpha X'' + \alpha^2 G) = \rho, \tag{38a}$$

$$\frac{\mathrm{d}\rho}{\mathrm{d}t} + l^2 \rho = -Rw. \tag{38b}$$

The analogue of (24) is

$$\frac{\mathrm{d}}{\mathrm{d}t}(\tilde{X}^2 + \epsilon^2)\frac{\mathrm{d}\hat{\rho}}{\mathrm{d}t} + (\tilde{X}\tilde{X}'' + \tilde{G})\,\hat{\rho} = 0, \tag{39}$$

where $\tilde{G} = R^{-1}G$.

With impulse forcing, solutions to (39) are made up of associated Legendre functions of order 0. Over the $n$th interval between impulses

$$\hat{\rho} = C_p^n P_{\nu_n}(\mathrm{i}R\tilde{X}) + C_q^n Q_{\nu_n}(\mathrm{i}R\tilde{X}), \tag{40a}$$

where

$$\nu_n = -\tfrac{1}{2} + (\tfrac{1}{4} - Ri_n)^{\frac{1}{2}}, \quad Ri_n = \frac{\tilde{G}}{X_n'^2}. \tag{40b}$$

When $Ri_n$ is greater than $\frac{1}{4}$, $\nu_n$ is of the form $-\frac{1}{2} + \mathrm{i}\nu_{1,n}$.

We now consider the model case of the two delta functions that was discussed in §4.2. For this case $Ri$ and $\nu$ are independent of $n$. The expressions for the Floquet factors are $\hat{\sigma} = \Lambda \pm (\Lambda^2 - 1)^{\frac{1}{2}}$. For no zero points

$$\Lambda = \bar{F}(PQ, 2\pi)\,\bar{F}(PQ, \pi) - \tfrac{1}{2}\bar{F}(P^2, 2\pi)\,\bar{F}(Q^2, \pi) - \tfrac{1}{2}\bar{F}(Q^2, 2\pi)\,\bar{F}(P^2, \pi), \tag{41}$$

and for two zero points

$$\begin{aligned}\Lambda = {} & \bar{F}(PQ, 2\pi)\,\bar{F}(PQ, \pi) - \tfrac{1}{2}\bar{F}(P^2, 2\pi)\,\bar{F}(Q^2, \pi) - \tfrac{1}{2}\bar{F}(Q^2, 2\pi)\,\bar{F}(P^2, \pi) \\ & + \pi\mathrm{i}\bar{F}(PQ, 2\pi)\,\bar{F}(P^2, \pi) - \pi\mathrm{i}\bar{F}(P^2, 2\pi)\,\bar{F}(PQ\,\pi) + \tfrac{1}{2}\pi^2\bar{F}(P^2, 2\pi)\,\bar{F}(Q^2, \pi),\end{aligned} \tag{42}$$

where

$$\bar{F}(PQ, t_n) = \left(\frac{\mathrm{d}}{\mathrm{d}\tau}(1 - \tau^2)\,P_\nu(\tau)\,Q_\nu(\tau)\right)\Bigg|_{\tau_n}, \quad \tau = \mathrm{i}R\tilde{X}. \tag{43}$$

The expressions are different for the two cases because connection formulae are needed for zero points. The argument of $Q_\nu$ then passes through that function's branch cut. The formulae are (Olver 1974)

$$C_p^{n,+} = C_p^{n,-} + \pi\mathrm{i}C_q^{n,-}, \quad C_q^{n,+} = C_q^{n,-}, \tag{44}$$

where the plus and minus superscripts refer to intervals with plus and minus $\tilde{X}$. Equation (44) indirectly indicates the destabilization effect of zero points. When $\nu$ is real and greater than $-\frac{1}{2}$, $Q_\nu$ is recessive at $\infty$ and $P_\nu$ is dominant.

The $\Lambda$ can be considerably simplified when $|\tau(\pi)|$ and $|\tau(2\pi)|$ are both large. Then, except when $\nu = -\frac{1}{2}$, when log terms enter,

$$P_\nu \approx \frac{2^\nu \pi^{-\frac{1}{2}}\Gamma(\frac{1}{2} + \nu)}{\Gamma(1 + \nu)}\tau^\nu + \frac{2^{-\nu-1}\pi^{-\frac{1}{2}}\Gamma(-\frac{1}{2} - \nu)}{\Gamma(-\nu)}\tau^{-\nu-1} = A\tau^\nu + B\tau^{-\nu-1}, \tag{45a}$$

$$Q_\nu \approx \frac{2^{-\nu-1}\pi^{\frac{1}{2}}\Gamma(1 + \nu)}{\Gamma(\frac{3}{2} + \nu)}\tau^{-\nu-1} = D\tau^{-\nu-1}. \tag{45b}$$

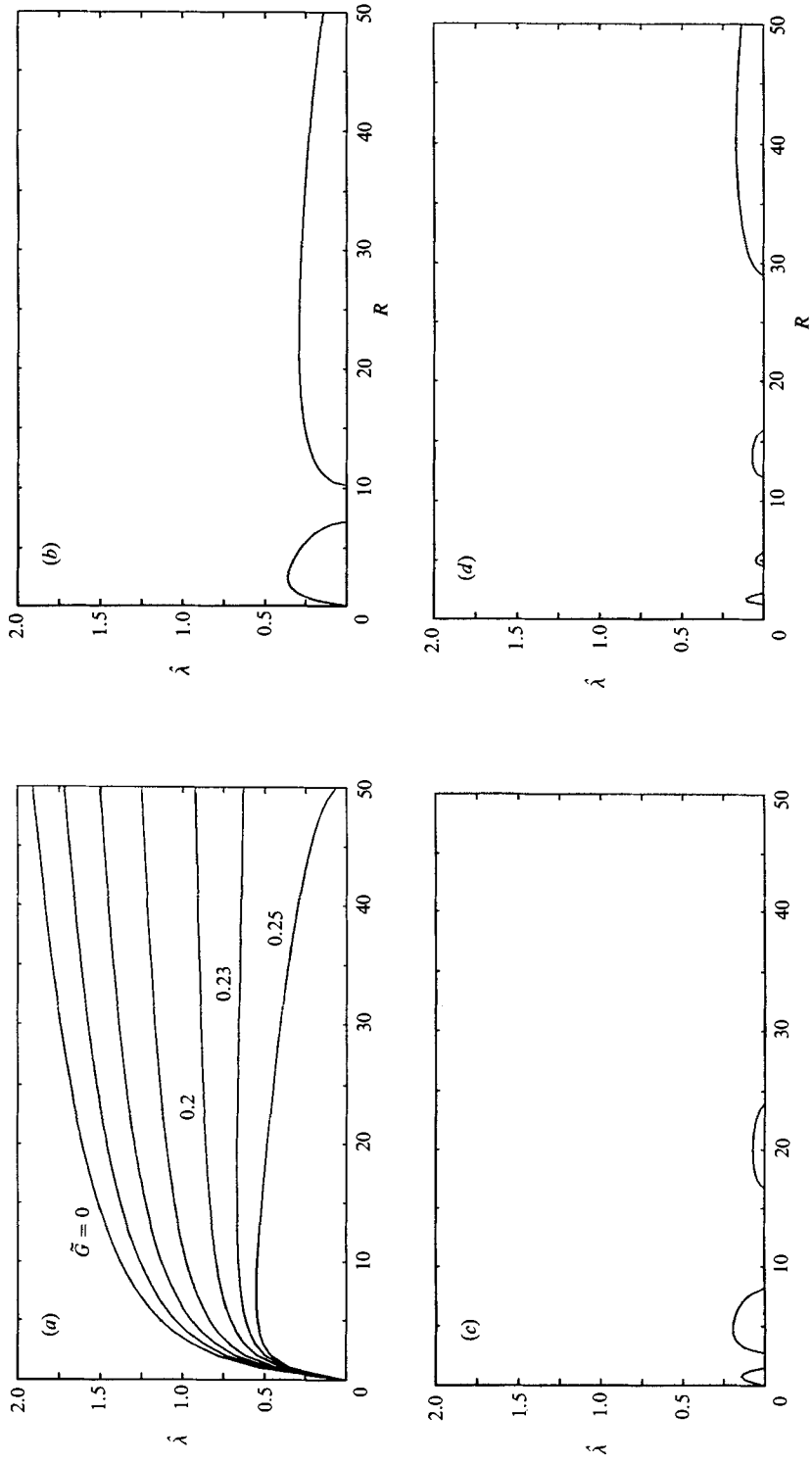


FIGURE 6. $\hat{\lambda}$ as a function of $R$ for (*a*) $\tilde{G} = 0$, 0.05, 0.10, 0.15, 0.20, 0.23, and 0.25; (*b*) $\tilde{G} = 0.30$; (*c*) $\tilde{G} = 0.40$; and (*d*) $\tilde{G} = 0.60$. $\tilde{X} = \cos t - 0.5$.

Two useful relationships between $A$, $B$, and $D$ are that $D = \pi \cot \pi\nu B$ and that $\pi \cot \pi\nu \, AB = 1/(2\nu+1)$.

We now consider (41) and (42) as $R \to \infty$. With no zero points, from (40*b*), (41), (45),

$$\Lambda \approx \frac{1}{1-4Ri}\left(1-4Ri\cosh\left(2(1-4Ri)^{\frac{1}{2}}\ln\left(\frac{\tilde{X}_{\max}}{\tilde{X}_{\min}}\right)\right)\right). \tag{46}$$

This gives weak subharmonic instabilities. With two zero points and for $Ri < \frac{1}{4}$

$$\Lambda \approx 2(\nu+1)^2 2^{4\nu}\frac{\Gamma^4(\frac{1}{2}+\nu)}{\Gamma^4(1+\nu)}(-\tilde{X}_{\max}\tilde{X}_{\min})^{2\nu+1}R^{4\nu+2}. \tag{47}$$

When $\nu = 0$ this reproduces the dominant term (with $\Psi$ approximated as $\pi$) of the $G = 0$ case. Equation (47) breaks down as $\nu \to -\frac{1}{2}$, since $\Gamma(\frac{1}{2}+\nu)$ then becomes infinite. A more complete expansion of (42) shows that as long as $\nu$ is real, the two-zero-point case gives instability growth rates that are a monotonically decreasing function of $Ri$. Once $Ri$ becomes greater than $\frac{1}{4}$, $\Lambda$ becomes oscillatory. $Ri = \frac{1}{4}$ is roughly the bound between strong and weak instabilities.

We briefly consider sinusoidal accelerations. Results are qualitatively in agreement with the impulse case. Figure 6 shows results for $\tilde{X} = \cos t - 0.5$. $\hat{\lambda}$ appears to steadily increase with $R$ for $\tilde{G}$ of up to about 0.21. Above that $\hat{\lambda}$ becomes oscillatory in $R$. Both subharmonic and harmonic instabilities are found. Also, there are regions of neutral ($\hat{\lambda} = 0$) untuned modes. These are especially prevalent for (figure 6*c*) $Ri = 0.4$. Above $\tilde{G} = 0.3$ instabilities are generally weak. Decay in $\hat{\lambda}$ with increasing $\tilde{G}$, however, is not monotonic. Figure 6(*d*) shows, for example, that $\hat{\lambda}$ has a peak at about $\tilde{G} = 0.6$. One slight difficulty with forcings other than the two-delta-function model is that $Ri$ is not constant. The values of $Ri$ that are probably most relevant to the instability process are the $Ri$ at zero points. For $\tilde{X} = \cos t - 0.5$, these are equal to $\frac{4}{3}\tilde{G}$.

## 6. Concluding comments

The work here has primarily considered the case of zero $G$. For this case, one significant result has been the demonstration of the relative weakness at large $R$ of the Kelvin–Helmholtz instability. The Rayleigh–Taylor instability then has a growth rate of $O(R^{\frac{1}{2}})$ while the Kelvin–Helmholtz growth rate is only $O(\ln R)$. This weakness should perhaps not have been entirely unexpected since the stability of uniform shear without density gradients is well known. Uniform shear precludes the existence of fast-growing inflectional instabilities. The shear's chief effect when it is large is to distort, disorganize, and thereby weaken any perturbations. Stretching of the wave by the shear also enhances viscous diffusion. On the other hand, at small $R$, this disorganizing effect is weak, and Kelvin–Helmholtz instabilities can then play a dominant role. The Kelvin–Helmholtz case remains unstable as $R \to 0$ while the Rayleigh–Taylor case has a finite $R_c$.

An important question is how applicable our Kelvin–Helmholtz results are to flows with boundaries. We have therefore begun to look at the case of oscillated flow between two parallel planes. Such a flow could be excited by oscillating a long container that has a fluid with a uniform temperature gradient between its top and bottom. The resulting parallel oscillating flow in the bulk of the container is then given by (3). We assume that the non-dimensional height $H$ of the container is $\gg 1$ and therefore that effects of $O(1)$-width top and bottom Stokes layers can, to a

first approximation, be ignored. With $\beta = Y'' = Z'' = G = 0$ the flow perturbation equations are

$$\left(\frac{\partial}{\partial t} - \tilde{\nabla}^2\right)\tilde{\nabla}^2 w = -\mathrm{i}\alpha X''(t)\left(\frac{\partial}{\partial z} - \mathrm{i}\alpha R X(t)\right)\rho, \tag{48a}$$

$$\left(\frac{\partial}{\partial t} - Pr^{-1}\tilde{\nabla}^2\right)\rho = -Rw, \tag{48b}$$

where

$$\tilde{\nabla}^2 = \left(\frac{\partial}{\partial z} - \mathrm{i}\alpha R X(t)\right)^2 - \alpha^2;$$

$\rho = 0$ at 0 and $H$. For $w$, both no-slip and no-stress boundary conditions have been considered.

Qualitative results can for the most part be understood in terms of the unbounded case. In the unbounded case, it was found that instability growth rates are greatest at $\gamma = 0$. Consistent with this, the preferred mode for the bounded case is very smooth in the vertical, of form $\sin(\pi z/H)$. $\partial/\partial z$ is thus $O(\pi/H)$. The case $\alpha R \gg \pi/H$ is particularly simple to understand. The growth, though not the structure, of the perturbation eigenfunction can then be understood from (48) with the $z$-derivatives set equal to zero. In other words, the eigenfunction's behaviour is given approximately by the unbounded equations (9) with $\gamma = 0$. At large $R$, eigenfunction growth, just as in the unbounded case, has been found to be concentrated at zero points. When $|\partial/\partial z| \ll |\alpha R|$ these zero points are (i) almost coincident with $X(t) = 0$ and (ii) occur almost simultaneously throughout $z$.

No systematic effort has yet been made to find critical $R$ as a function of $H$. Unlike the unbounded case, the damping effects of a necessarily finite $\partial^2/\partial z^2$ makes $R_c$ greater than zero. It is worth noting, however, that $R_c$ can still be very small. For example, with $H = 100$ (for water with $\omega = 1$ the corresponding dimensional height is, typically, less than 10 cm) instabilities have been found for $R$ down to 0.07.

## REFERENCES


Arscott, F. M. 1964 *Periodic Differential Equations*. Macmillan.

Bayley, B. J. 1986 Three-dimensional instability of elliptical flow. *Phys. Rev. Lett.* **57**, 2160.

Bellman, R. 1953 *Stability Theory of Differential Equations*. McGraw-Hill.

Burde, G. I. 1970 Numerical investigation of convection arising in a modulated field of external forces. *Izv. Akad. Nauk SSSR Mzhg* **5**, 196.

Craik, A. D. D. 1989 The stability of unbounded two- and three-dimensional flows subject to body forces: some exact solutions. *J. Fluid Mech.* **198**, 275.

Craik, A. D. D. & Criminale, W. O. 1986 Evolution of wavelike disturbances in shear flows: a class of exact solutions of the Navier–Stokes equations. *Proc. R. Soc. Lond.* A **406**, 13.

Donnelly, R. J., Reif, F. & Suhl, H. 1962 Enhancement of hydrodynamic stability by modulation. *Phys. Rev. Lett.* **9**, 363.

Farrell, B. F. 1989 Transient development in confluent and diffluent flows. *J. Atmos. Sci.* **46**, 3279.

Gresho, P. M. & Sani, R. L. 1970 The effects of gravity modulation on the stability of a heated fluid layer. *J. Fluid Mech.* **40**, 783.

Hall, P. 1978 The linear stability of flat Stokes layers. *Proc. R. Soc. Lond.* A **359**, 151.

Hartman, R. J. 1975 Wave propagation in a stratified shear flow. *J. Fluid Mech.* **71**, 89–104.

Howard, L. N. 1961 Note on a paper of John W. Miles. *J. Fluid Mech.* **10**, 509.

Kamotani, Y., Prasad, A. & Ostrach, S. 1981 Thermal convection in an enclosure due to vibrations aboard spacecraft. *AIAA J.* **19**, 511.

KERCZEK, C. VON & DAVIS, S. H. 1974 Linear stability theory of oscillatory Stokes layers. *J. Fluid Mech.* **62**, 753.

KERCZEK, C. VON & DAVIS, S. H. 1976 The instability of a stratified periodic boundary layer. *J. Fluid Mech.* **75**, 287.

LAGNADO, R. R., PHAN-THIEN, N. & LEAL, L. G. 1984 The stability of two-dimensional linear flows. *Phys. Fluids* **27**, 1094.

LANDMAN, M. J. & SAFFMAN, P. G. 1987 The three-dimensional instability of strained vortices in a viscous fluid. *Phys. Fluids* **30**, 2339.

MARCUS, P. S. & PRESS, W. H. 1977 On Green's functions for small disturbances of plane Couette flow. *J. Fluid Mech.* **79**, 525.

MOORE, R. A. 1956 The least eigenvalue of Hill's equation. *J. Analyse Math.* **5**, 183.

OLVER, F. W. J. 1974 *Asymptotics and Special Functions.* Academic.

STOKER, J. J. 1950 *Nonlinear Vibrations.* Interscience.

THOMSON, W. 1887 Stability of fluid motion: rectilinear motion of viscous fluid between two parallel plates. *Phil. Mag.* **24**, 188.

TUNG, K. K. 1983 Initial value problems for Rossby waves in a shear flow with critical level. *J. Fluid Mech.* **133**, 443.

WADIH, M. & ROUX, B. 1988 Natural convection in a long vertical cylinder under gravity modulation. *J. Fluid Mech.* **193**, 391.